Plasmonics (2022) 17:1489–1500
https://doi.org/10.1007/s11468-022-01639-2

# Sensitive Detection of SARS-CoV-2 Using a Novel Plasmonic Fiber Optic Biosensor Design

Yosra Saad[1] · Mohamed Hichem Gazzah[1] · Karine Mougin[2] · Marwa Selmi[3] · Hafedh Belmabrouk[3]

Received: 28 December 2021 / Accepted: 11 April 2022 / Published online: 23 April 2022


## Abstract

The coronavirus (COVID-19) pandemic has put the entire world at risk and caused an economic downturn in most countries. This work provided theoretical insight into a novel fiber optic-based plasmonic biosensor that can be used for sensitive detection of SARS-CoV-2. The aim was always to achieve reliable, sensitive, and reproducible detection. The proposed configuration is based on Ag-Au alloy nanoparticle films covered with a layer of graphene which promotes the molecular adsorption and a thiol-tethered DNA layer as a ligand. Here, the combination of two recent approaches in a single configuration is very promising and can only lead to considerable improvement. We have theoretically analyzed the sensor performance in terms of sensitivity and resolution. To highlight the importance of the new configuration, a comparison was made with two other sensors. One is based on gold nanoparticles incorporated into a host medium; the other is composed of a bimetallic Ag-Au layer in the massive state. The numerical results obtained have been validated and show that the proposed configuration offers better sensitivity (7100 nm\RIU) and good resolution (figure of merit; FOM = 38.88 $RIU^{-1}$ and signal-to-noise ratio; SNR = 0.388). In addition, a parametric study was performed such as the graphene layers' number and the size of the nanoparticles.

**Keywords** Surface plasmon resonance (SPR) · SARS-CoV-2 · Ag–Au alloy nanoparticles · Graphene layer · Optical fiber · COVID-19

## Introduction

The new coronavirus illness 2019 (COVID-19) is induced by hard acute respiratory syndrome coronavirus 2 (SARS-CoV-2) infection and continues to be a grave threat to global human health and the global economy. This virus can be quickly transmitted from human to human via different media, such as nearby interpersonal contacts, airborne droplets, and fomites [1, 2]. The development of a sensitive, specific, and rapid diagnostic tool for SARS-CoV-2 infection is certainly supportive of the control of the infection transmission. For this reason, important research efforts have focused on early management and the development of several diagnostic methods such us serological immunological assays (ELISA, CGIA, enzyme-linked immunosorbent assay, colloid gold-based immunochromatographic assay) [3, 4], chest computed tomography (CT) [5], and reverse transcription polymerase chain reaction (RT-PCR) [6, 7]. Nevertheless, RT-qPCR needs at least 3 h and demands sophisticated testing setups [8] in addition to suffering from false positives. To this end, one potential area is the use of biosensors [9, 10].

In the near future, miniaturized real-time molecular detection devices will be at the center of the revolution in methods of medical diagnostics and identification of biological processes, both at the clinical level and at the research level. Fiber optic biosensors based on the surface plasmon resonance (SPR) phenomenon have become indispensable tools for sensitive, unmarked, and real-time detection of

✉ Yosra Saad
yosra_saad@yahoo.com

[1] Laboratory of Quantum and Statistical Physics, Faculty of Sciences of Monastir, University of Monastir, 5019 Monastir, Tunisia

[2] University of Haute-Alsace, Institute of Materials Science of Mulhouse, IS2M-CNRS-UMR 7361, 15 Rue Jean Starcky, 68057 Mulhouse, France

[3] Laboratory of Electronics and Microelectronics, Faculty of Science of Monastir, University of Monastir, 5019 Monastir, Tunisia

biological and biochemical interactions [11, 12] especially for the detection of SARS-CoV-2 [13, 14].

These sensors are extremely powerful detection tools, useful for a large variety of applications in several fields such as biomedical research, healthcare system, pharmaceutical industry, and many others [15–17]. Despite their contributions in several fields, conventional plasmonic sensors based on the use of a flat metal surface of gold are limited in terms of sensitivity, especially when it comes to detecting molecules of low molar masses. It is in this problematic context that this work is situated. This work mainly consists of a numerical study of nanostructured plasmonic metal surfaces in order to study their potential application as optical biosensors. Indeed, these structures have new properties in their interaction with light and can more efficiently excite surface plasmons.

Metallic nanoparticles (NPs) have received great attention in recent years [18–20], due to their unique properties. These properties depend on the size and shape and are markedly different from those of massive material [21–23]. A nanoparticle is a set of polyatomic structures varying in size between 1 and 100 nm [18]. For several decades, gold has been considered an inert material in a massive state, but at the nanoscale, it has very unusual properties: optical, electronic, photonic, magnetic, and catalytic. These intrinsic properties of nanoparticles are due to a quantum confinement effect, the high reactivity of surface electrons, to their small sizes, their geometric architecture, and also to their surface structures [24, 25]. This is the reason why the research in this work aims to improve conventional sensors by using metallic NPs instead of massive metallic film.

Different metallic nanostructures have been used in the SPR biosensor. Gold is the preferred metal in most commercial SPR sensors due to its chemical stability and its high biocompatibility despite having a relatively wide resonance peak [26]. While silver offers the best resolution and a narrow resonance peak, it however degrades rapidly by oxidation. Thus, a new structure of the metallic layer has been the subject of different studies in order to couple the advantages of both noble metals [27]. This is the Ag-Au bimetallic structure.

The concept of bimetallic has attracted considerable attention as an effective approach in the development of SPR sensors. However, an alloy-based configuration of the Ag-Au bimetallic nanoparticles is able to demonstrate more effective optical characteristics than pure gold or pure silver. To take advantage of the benefits of NPs, the sensitivity of gold, and its stability over time as well as the higher SNR value obtained with silver NPs, we have proposed in this article to study a biosensor fiber optic SPR based on the alloy of Ag-Au bimetallic NPs. To highlight the importance of the proposed new structure, we compared it with two different configurations. One is based on gold nanoparticles incorporated into a host medium; the other is composed of a bimetallic layer in the uniform state.

It is known that the functionalization of the surface is a key step for the production of the biosensor and therefore for obtaining good analytical performance. Indeed, improving the performance of biosensor characteristics requires improving the absorption of biomolecules. Hence, the nature of the surface on which biological molecules are adsorbed plays a key role. The drawback of metals is that they are poor biomolecular adsorbents [28] which decrease the sensitivity and selectivity of the biosensor. Furthermore, direct ligand immobilization on a metal surface could distort them, which would lead to a negative effect on molecular interactions [29]. To overcome these limitations, various strategies in the literature have been investigated using additional flat film layers such as dielectric layers, thiol acid [30], ITO [31], and TiO2 [32] layer.

Recently, graphene has attracted the attention of researchers as another approach to improve the sensitivity of several categories of sensors [33]. Indeed, graphene has very interesting optical characteristics. The graphene monoatomic thickness in addition to broadband absorption and optical transparency affords a good platform for electro-optical devices. Interband and inband electronic transitions are the principal mechanisms behind the broadband optical absorption of graphene [34, 35]. Thus, graphene can be used as a biomolecular immobilizing layer allowing the increase of the absorption efficiency of the bio-recognition molecules on the surface of the biosensor because of $\pi$-stacking type interactions [36] between the cycles of graphene and those of biological molecules. This is why the graphene has received a great deal of attention. In our previous work, we used a graphene layer as a protective layer, which also serves to improve the sensitivity of the SPR sensor to reach a maximum equal to 7000 nm\RIU [33]. In addition, Ahmmed A Rifat et al. [37] has also studied a configuration based on graphene coated on a silver film to protect it against oxidation and improve molecular adsorption. This has resulted in improving sensor performance, allowing reaching a sensitivity equal to 3000 nm/RIU.

In the current study, in order to raise the performance of fiber optical SPR sensor in terms of sensitivity and resolution, a layer of graphene has been applied to the Ag-Au NPs alloy film. To our knowledge, such a configuration has never been carried out. Here, graphene is considered an element of biorecognition thanks to its various and multiple properties. We then compared this new configuration to the other two sensors. One is based on gold NPs incorporated in a host medium; the other is based on a bimetallic layer in the massive and uniform state. This comparison reflects the importance and utility of the alloy which serves to couple the advantages of two metals in nanoscale state in a single configuration better than using pure gold or pure silver. We obtained as a result an increase in the sensitivity and the

resolution (figure of merit and SNR) of the sensor. A parametric study was subsequently performed such as the effect of nanoparticle size and the graphene layer number effect. Motivated by such excellent characteristics of this biosensor design, we proposed to apply it on SARS-CoV-2 detection. We think that the suggested biosensor has a great potential to recognize SARS-CoV-2 accurately and rapidly in practical clinical applications.

## Design Consideration and Theoretical Model

The principle of an SPR sensor is to couple the incident light with the surface plasmons. Remember that these plasmons are quantified and collective oscillations of free electrons at the interface of a metal and a dielectric. This coupling can be caused by total reflection of an optical wave injected on the opposite interface. The evanescent field crossing the metal layer permits the surface plasmon excitation at the metal/dielectric interface. The so-called ATR (attenuated total reflexion) process is the most widely used for the excitation of surface plasmons. It was put into practice for the first time by A. Otto then by E. Kretshmann who used a prism as a coupler [38]. During the last decade, the use of optical fibers as a coupler has emerged in different forms thanks to the advantages they have offered. In this study, we were interested in the fiber optical SPR sensor in a new configuration. As shown in Fig. 1, the suggested biosensor is founded on a film made from an alloy of Ag/Au nanoparticles topped with a layer of graphene (Fig. 1a). This plasmonic biosensor can be used for the SARS-CoV-2 detection. Thiol-attached DNA is employed as a ligand layer for the detection medium because it has displayed great properties as a receptor for SARS-Cov-2 as shown in (Fig. 1c) [39, 40]. Figure 1b shows gold nanoparticles embedded in a host material.

In order to build experimentally a sensing surface on the optical fiber, the cladding was chemically removed. This bare part was covered with a metal film based on Ag-Au nanoparticle alloy followed by a graphene layer. Once the fiber is ready, a white light source is connected to the input side of the fiber which is immersed in a cell where a series of analyte solutions will be injected. A spectrometer coupled to the fiber records the transmission of the light as it leaves the fiber [41, 42]. The light beam crosses the detection area of the fiber and excites

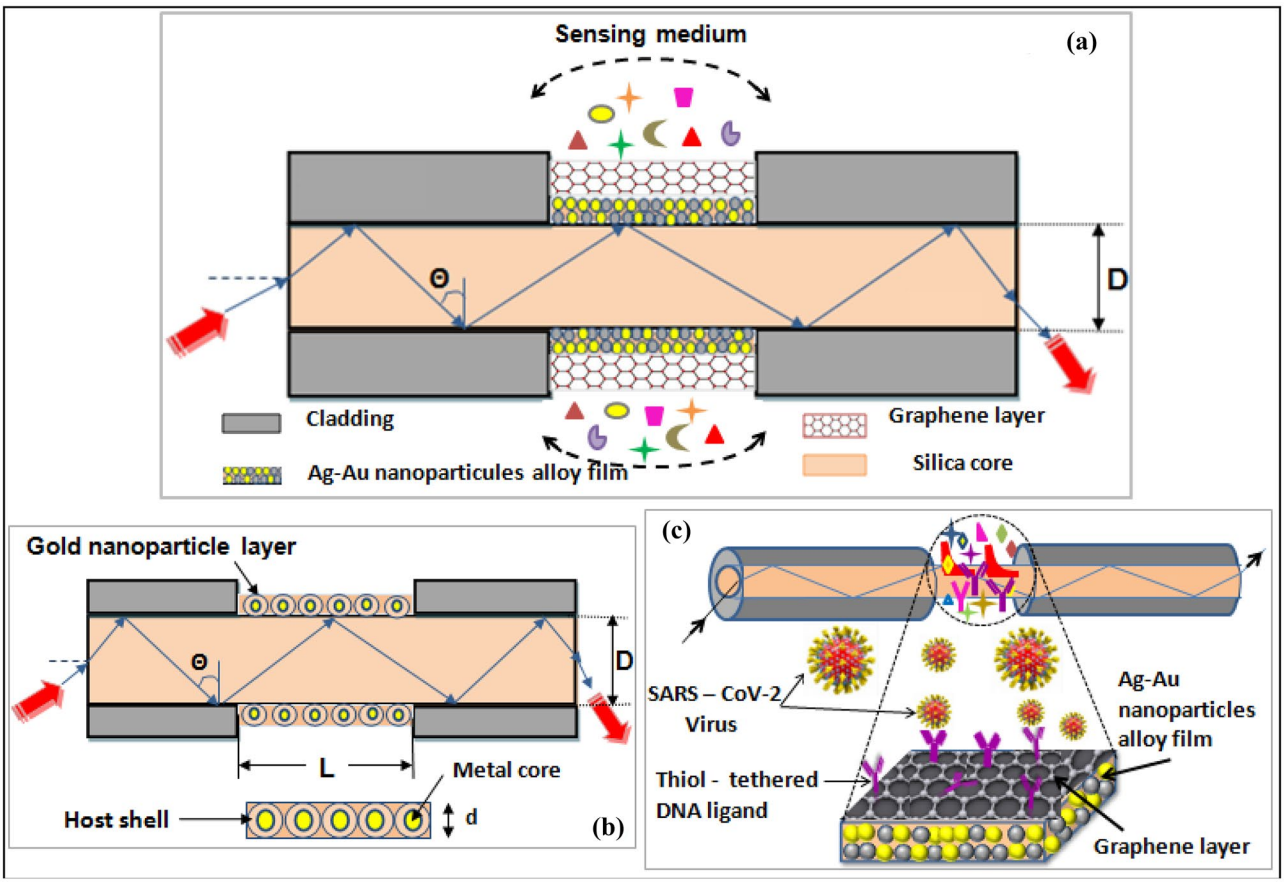


**Fig. 1** structural sensor design; **a)** configuration based on an alloy film of Ag-Au spherical nanoparticles covered with a layer of graphene, **b)** Configuration based on gold nanoparticles incorporated into a host medium, **c)** SARS-CoV-2 detection principle

the surface plasmons on the metal film, which causes a dip in the transmission spectrum called SPR curve.

The equations having been implemented using Matlab software, we then had to define the numerical values for the simulation.

## The Silica Core of the Optical Fiber

We considered the core of the multimode fiber to be molten silica. The expression of the Refraction index is written in the following form according to the Sellmeier relation [43]:

$$n(\lambda) = \sqrt{1 + \frac{A_1\lambda^2}{\lambda^2 - B_1^2} + \frac{A_2\lambda^2}{\lambda^2 - B_2^2} + \frac{A_3\lambda^2}{\lambda^2 - B_3^2}} \quad (1)$$

$\lambda$ is the wavelength expressed in micrometers. $A_1 = 0.696\ 1663$; $A_2 = 0.877\ 4794$; $A_3 = 0.407\ 9426$; $B_1 = 0.068\ 4043$; $B_2 = 9.896\ 161$; $B_3 = 0.116\ 2414$

## Au–Ag Alloy Nanoparticle Film

The metallic medium dielectric function has been adjusted by the classic Drude function [44]:

$$\varepsilon(\omega) = \varepsilon^{\infty} - \frac{\omega_p^2}{\omega(\omega + i\omega_d)} \quad (2)$$

$\varepsilon^{\infty}$ is the dielectric constant at infinite frequency and $\omega_p$;$\omega_d$ are the plasma and damping pulses respectively. These pulsations are expressed in the following form:

$$\omega_p^2 = \frac{Ne^2}{m\varepsilon_0} \quad (3)$$

and

$$\omega_d = \frac{v_f}{R_{bulk}} \quad (4)$$

where $m$, $e$, and $N$ are the effective mass, concentration, and charge of free electrons, respectively; $R_{bulk}$ defines the conduction electrons average free path in bulk metal, and $v_f$ defines the electrons speed at the Fermi energy.

The conduction electrons are dispersed by the surface when the particle size, $R$, is less than the average free path in the bulk metal. Therefore, the mean free path, $R_{\text{eff}}$, of the electrons becomes dependent on the particle size following this relationship:

$$\frac{1}{R_{eff}} = \frac{1}{R} + \frac{1}{R_{bulk}} \quad (5)$$

This equation has been experimentally justified for gold and silver particles as small as 2 nm [45].Thus, the damping pulsation is expressed by:

**Table 1** Parameters of gold and silver nanoparticles

| Parameter | Gold | Silver |
|---|---|---|
| Plasma frequency,$\omega_p(rad.s^{-1})$ | $1.40 \times 10^{16}$ | $1.35 \times 10^{16}$ |
| Damping frequency,$\omega_d(bulk)(rad.s^{-1})$ | $3.78 \times 10^{13}$ | $7.62 \times 10^{13}$ |
| High frequency dielectric constant,$\varepsilon^{\infty}$ | 7.0 | 2.48 |
| Fermi velocity,$v_f(m.s^{-1})$ | $1.40 \times 10^{6}$ | $1.40 \times 10^{6}$ |

$$\omega_d(R) = \omega_d(bulk) + \frac{\vartheta_f}{R} \quad (6)$$

Equation (2)+(3), (4), and (6) illustrate the dielectric function which depends on the size of a metal particle. Silver and gold NPs are assumed to be spherical in shape. For the $Ag_yAu_{1-y}$ alloy, the dielectric constant can be supposed to depend on the composition-weighted average of the dielectric constants Ag and Au and is defined by [46]:

$$\varepsilon_A(y,\omega) = y\varepsilon_{Ag}(\omega) + (1-y)\varepsilon_{Au}(\omega) \quad (7)$$

Here, $y$ is the silver NP volume fraction. The parameters of gold and silver nanoparticles are summarized in Table 1.

The manufacture of the bimetallic alloy of nanoparticles exists and has been investigated in detail. In fact, there are two manufacturing methods. The first is the multi-layer method, i.e., the alloy film is composed of several thin layers of two metals [46]. The second method consists of mixing the NPs of two metals in the required proportions. In fact, such an Ag-Au alloy is made with sequential spraying and co-reduction of chloroauric acid ($HAuCl_4$) and silver nitrate ($AgNO_3$) with sodium citrate [47]. Nevertheless, in both techniques, the dielectric constant of the bimetallic alloy film varies with the composition-weighted average of the dielectric constants as shown in Eq. (7).

Au colloidal NPs used in the study ranged form few nanometers to several tens of nanometers in size and had a polyhedral structure with well-defined facets (Fig. 2). The most common particle shapes were pentagonal dipyramids and octahedrons [48].

The synthesis of "bare" Au NPs, described in more details in the experimental section, involved the addition of sodium citrate [49].

## Nanoparticles Incorporated in a Host Medium

Based on Maxwell–Garnett theory, the effective dielectric function ($\varepsilon_{eff}$) of a material composed of great volume fraction metal nanoparticles incorporated isotropically in a non-absorbent medium is expressed by the following equation:

$$\varepsilon_{eff} = \varepsilon_m\left(1 + \frac{3\varnothing\beta}{1 - \varnothing\beta}\right) \quad (8)$$

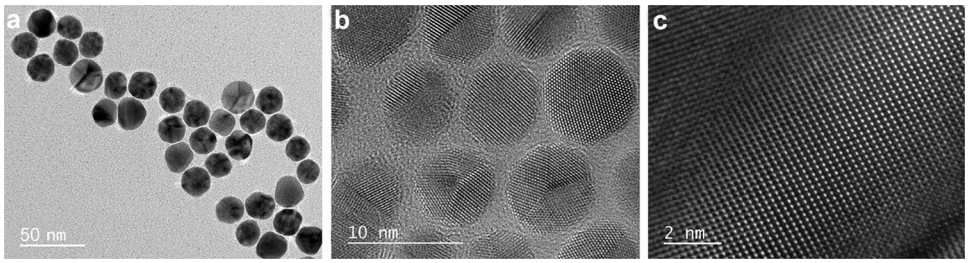


**Fig. 2** TEM images of Au NPs that tend to have a polyhedron-like shape **a** 30 nm diameter Au NPs, **b** 5 nm diameter Au NPs, **c** zoom in on a NP to visualize the high organization of Au atoms in the NP

where

$$\beta = \frac{\varepsilon - \varepsilon_m}{\varepsilon + 2\varepsilon_m} \tag{9}$$

$\varepsilon_m$ is the dielectric function of the host medium in which the gold NPs are incorporated. ∅ is the volume ratio of the embedded particles.

The metal particle volume ratio can be provided by Ung et al. [50]:

$$\varnothing = \frac{0.74R^3}{(R + R_{host})^3} \tag{10}$$

where $R_{\text{host}}$ is the thickness of the silica shell. The film thickness depends on the cycle number deposited. Each cycle can be represented by the deposition of a monolayer of particles.

## Graphene Layer

The refractive index of graphene is expressed by the following expression [51]:

$$n_g = 3 + i\frac{c\lambda}{3} \tag{11}$$

where $\lambda$ is the wavelength in μm and $c \approx 5.446\mu m^{-1}$

## SARS-CoV-2 Biosensing: Sensing Layer

The last layer before the sensing medium is the thiol-tethered DNA. The data for refractive index versus thickness are taken from experimental results [52]. To expand an exact estimate of the mechanism of COVID-19 biosensing operation, a simulation model must first be conceived. Here, in a suggested model, COVID-19 is estimated to be a solid sphere core that contains RNA coated by a membrane protein with radiuses of $r_1$ and $r_2$, respectively [53]. Therefore, the virus effective R.I is determined by considering the two refractive indices volume-weighted sum:

$$n_{eff} = \frac{n_1 V_1}{V_1 + V_2} + \frac{n_2 V_2}{V_1 + V_2} = \frac{n_1 + n_2(\eta^3 - 1)}{\eta^3}; r_2 = \eta r_1 \tag{12}$$

where $n_1(V_1)$ and $n_2(V_2)$ are the RNA total R.I and the volume of the membrane protein, respectively. As the virus R.I is governed principally by material composition instead of its geometrical size, $\eta$ is a constant value for the virions same kind $\eta = 1.25$ [53]. The RNAs R.I average is 1.54 [54] and the refractive index of membrane proteins ranges from $1.46 + / - 0.006$ [55]. The average viral load is $7 * 10^6$ per ml, whereas the maximum is $2.35 * 10^9$ per ml [56]. When the sample is passed through the detection channel, COVID-19 RNA is bound to thiol-attached DNA. It needs some time to accumulate from the surface density of the virus. The standard waiting time is 10 s.

Note that the SARS-CoV-2 can be solved in a run buffer consisting of 10 mM HEPES and 120 mM NaCl solution. Indeed, the running buffer R.I can be measured experimentally by an optical sensor. When different concentrations of HEPES solution were mixed with 120 mM NaCl solution, there exists a good linear relationship between the running buffer refractive index and the HEPES concentration ranging from 0 to 120 mM, which can be expressed as: [57]

$$y = 0.00004x + 1.3341 \tag{13}$$

where $y$ and $x$ are the R.I of the running buffer and HEPES solution (mM), respectively. In this work, the HEPES solution concentration is 10 mM, so the sensing medium refractive index (R.I) was supposed to be 1.3345 [13].

## The Power Transmitted by the Optical Fiber

The principle of calculation followed in this work is founded on a multilayer system. The reflection coefficients were determined based on the matrix method adapted to a multilayer structure [58]. This method allows us to study the electromagnetic wave interaction for a precise number of layers and to determine the magnetic field $H_k$ and the electric field $E_k$ in the N layers.

When a light ray is focused on the entry face of an optical fiber, it undergoes refraction or reflection in the plane of incidence. The refracted ray then comes to reflect or refract at the core/cladding interface. A light ray must undergo total

reflection on the core/metal separation surface in order to excite a surface plasmon. There is therefore a total reflection if the incidence angle is greater than the critical angle $\theta_{cr}$ [33].

The calculation of the power transmitted by the optical fiber is linked by the reflectance $R_{\text{ref}}$ of the ray reflected at the core/metal interface and the reflection number that the light ray will undergo:

$$T = (R)^{N_{ref}(\theta)} \tag{14}$$

$$\text{where } N_{ref}(\theta) = \frac{L}{Dtan\theta} \tag{15}$$

$(\theta)$ is the angle of propagation, $D$ is the core diameter, and $L$ is the length of the sensitive layer.

The power, dP, exiting the fiber between the angles $\theta_0$ and $\theta_0 + d\theta_0$ and using Snell's law, is proportional to:

$$dP\alpha \frac{n_c^2 sin\theta cos\theta}{(1 - n_c^2 cos^2\theta)^2} d\theta \tag{16}$$

The light source used is unpolarized and collimated, so the transmitted and normalized light power is written in the following form:

$$T = \frac{\int_{\theta_{cr}}^{\pi/2} R^{N_{ref}(\theta)} P(\theta) d\theta}{\int_{\theta_{cr}}^{\pi/2} P(\theta) d\theta} \tag{17}$$

The SPR excitation is done with the intervention of, only, half of the injected power. So the expression of the transmission is written as follows:

$$T = \frac{1}{2}\left(\frac{\int_{\theta_{cr}}^{\pi/2} R^{N_{ref}(\theta)} P(\theta) d\theta}{\int_{\theta_{cr}}^{\pi/2} P(\theta) d\theta} + 1\right) \tag{18}$$

## Results and Discussions

To highlight the importance of the use of Au–Ag alloy nanoparticles in the SPR sensor, we compared its plasmon response with that of two SPR sensors. One is based on gold nanoparticles embedded in a host medium; the other is based on a massive Ag-Au bimetallic layer. The responses are simulated for a sensor with a sensitive length of 20 mm, a fiber core diameter of 600 µm, a metal layer of thickness equal to 55 nm, and the fraction volume of silver $y = 0.75$. The sensitive medium refractive index (RI) is equal to 1.34. Figure 3 presents the variation in transmission with wavelength for the three sensors respectively. It is clearly remarkable that the depth, transmission (94.7; 91.2; 95.9), full width at half maximum FWHM (55 nm; 39 nm; 58 nm), and resonant wavelength (555 nm; 571 nm; 602 nm) vary with the variation of the configuration involved. It appears that the proposed configuration has the narrowest curve also offering better resolution (curve in red). We can conclude that the best compromise between the full width at half maximum (FWHM), amplitude, and position of the resonance can be obtained for this configuration.

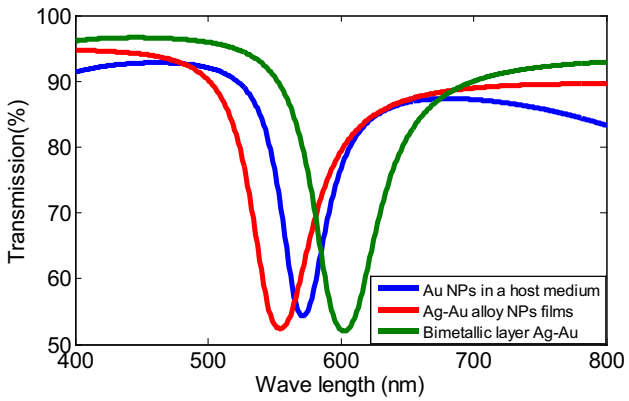


**Fig. 3** variation of the transmitted power as a function of the wavelength for the three configurations

The curves obtained in this work coincide well with that found by Sharma et al. [43] for a configuration based on the alloy of metallic nanoparticles. The appearance and general shape of the curves are comparable especially at the level of the minimum absorption ($\lambda_{res} = 555nm$). A slight difference can be explained by the difference between the parameters used. This justifies the validity of our numerical work.

Thanks to its interesting optical properties and especially its good absorption of molecules, a layer of graphene was added to the alloy film of Ag-Au nanoparticles in this work. This allows us to improve the performance of the SPR biosensor in terms of sensitivity and resolution.

The sensitivity shows the displacement of the plasmon resonance peak (augular or spectral) per unit of refractive index (RIU). It is defined by the following expression [31]:

$$S = \frac{\delta\lambda_{res}}{\delta n}(nm/RIU) \tag{19}$$

To better assess the sensitivity of detection, it is necessary to consider another parameter; the full width at half maximum of the SPR signal denotes FWHM. This increases with the value of the refractive index of the dielectric, inducing a larger SPR signal. By dividing the value of $S$ by the FWHM, we introduce the notion of «Figure of Merit (FOM)»

$$FOM = \frac{S}{FWHM} \tag{20}$$

The SPR sensor resolution can be described as the smallest change in refractive index that can be detected by a visible shift in the plasmon signal resonance wavelength. This parameter can be determined by the measurement of the limit of detection (LOD) or via the signal-to-noise ratio (SNR). The latter is strongly dependent on the resonance peak width. It is defined in the following form [31]:

$$SNR = \left[\frac{\delta\lambda_{res}}{\delta\lambda_{1/2}}\right]_n \tag{21}$$

Figure 4 presents a comparison of the sensitivity obtained for each configuration. The R.I of sensitive medium covers the range of indices between 1.32 and 1.40. The thickness of a graphene layer is 0.34 nm. It is noted from this figure that the sensitivity rises according to the R.I of the medium to be detected for the three configurations but it is not in the same way. In fact, the sensitivity obtained with an SPR biosensor based on an Ag-Au/graphene nanoparticle alloy is higher than the other two. It went from 1900 nm/RIU to 7100 nm/RIU while the sensitivity of the massive bimetallic configuration reaches a maximum equal to 6700 nm/RIU and the maximum sensitivity obtained by the configuration based on nanoparticles incorporated in a host medium is equal to 3300 nm/RIU. This improvement in sensitivity, on the one hand, is due to the fact that the Ag-Au nanoparticle alloy has more useful optical properties than pure gold or pure silver. This is related to the characteristics of the material, i.e., its nature, crystal structure, and state, since the coupling and the excitation of surface plasmons are based on the free electrons of the metal layer. In addition, the optical response is relatively important since the wavelength is large compared to the size of the nanoparticles. On the other hand, this increase in sensitivity can also be explained by the optical absorption efficiency of graphene especially the large imaginary part of its refractive index. In fact, the real part of the refractive index is related to the wave propagation while the imaginary part is related to the light absorption. Such a graphene layer improves, in the practical field, the adsorption and the molecular binding on the sensor surface. This allows to take advantage of the sensitivity, while maintaining the chemical stability of the sensor in the field with a graphene surface layer.

Such a sensor represents the combination of the advantages of metallic nanoparticles and graphene could only be the basis for the birth of an effective early detection system. Therefore, Fig. 5 illustrates the FOM variation with the sensitive medium refractive index. This parameter is used to analyze the overall SPR sensor performance. Thus, for the same variation of index, if the FOM is high, it indicates a large spectral shift of the signal or a narrower plasmonic signal, i.e., less error in the determination of the resonance wavelength. In both cases, this translates into better sensor performance. According to Fig. 5, the configuration based on an alloy film of the Ag-Au NPs has the highest FOM values when compared with the other two configurations. The maximum value of FOM reached by this configuration is equal to $38.88 RIU^{-1}$.

Figure 6 illustrates the evolution of SNR according to the RI of the medium to be detected for the three sensors. SNR

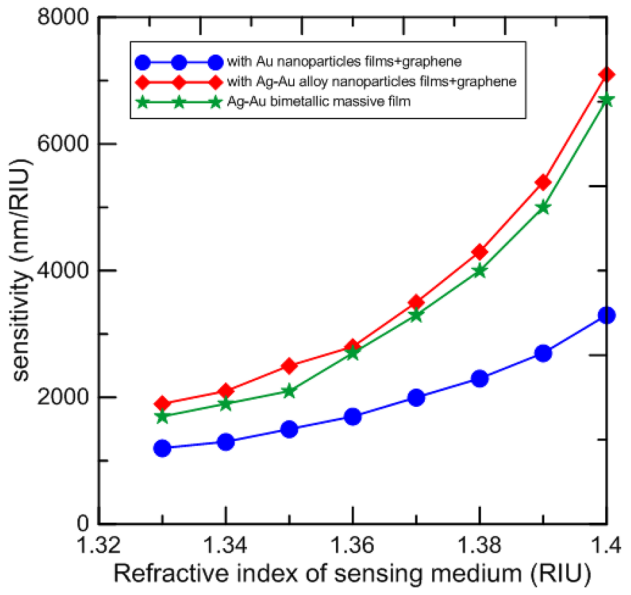


**Fig. 4** Variation of sensitivity depending on the sensing medium refractive index

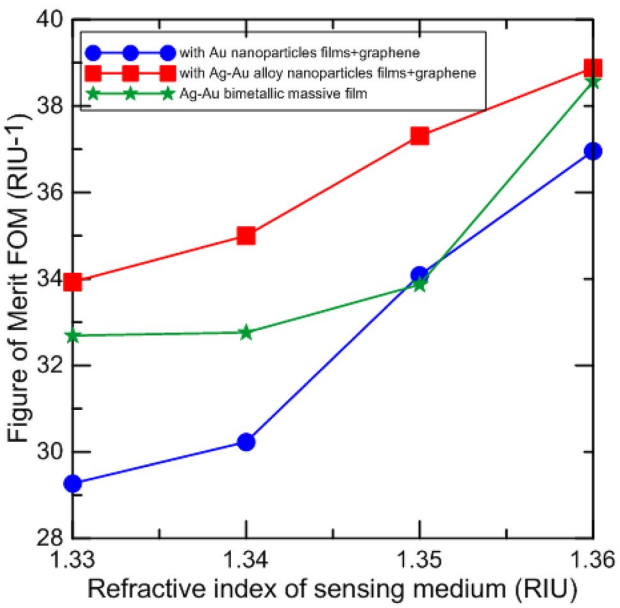


**Fig. 5** Variation of FOM with the sensing medium refractive index

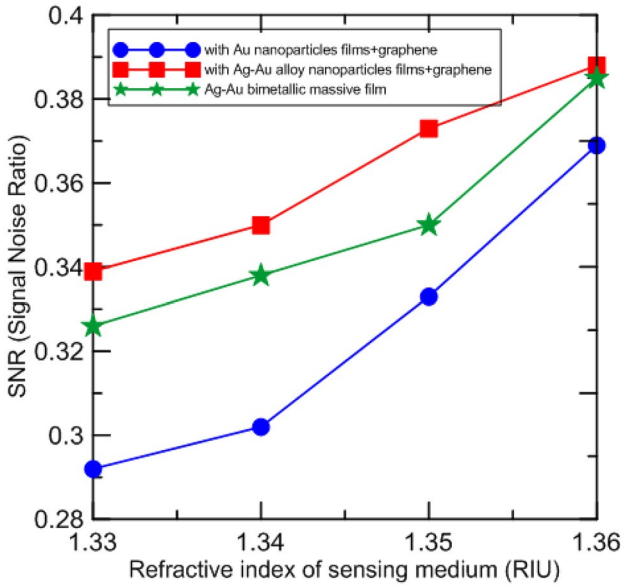


**Fig. 6** SNR variation according to the refractive index of the medium to be detected

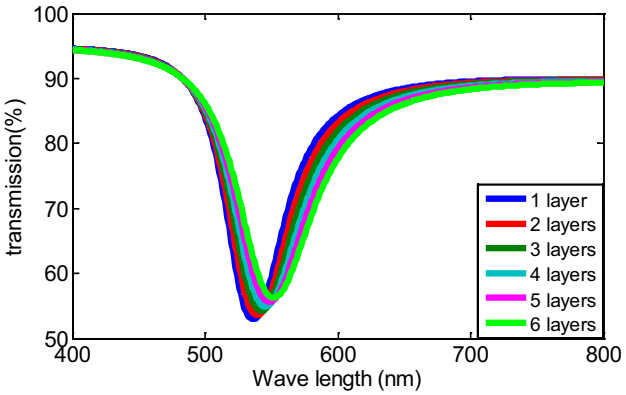


**Fig. 7** Effect of the graphene layer number on the SPR response of the sensor

increases with increasing refractive index. The best SNR is obtained with the proposed configuration based on an alloy of Ag-Au nanoparticles/graphene. The curve increases until it reaches a maximum value equal to 0.388, while the maximum SNR obtained with the sensor based on gold nanoparticles incorporated in a host medium and the sensor based on a bimetallic layer are 0.369 and 0.385 respectively. Therefore, the studied sensor offers the best resolution; in fact, the greater the SNR value is, the more precise the detection will be.

By comparing it with other works in the literature as shown in Table 2, we found that the obtained value of the sensitivity (7100 nm\RIU) is greater than those obtained with the previous configurations of the SPR sensors. It is evident that the proposed configuration could be used in a wide range of great sensitivity applications such as biological and biochemical detection.

The control of the graphene layer number transferred to the metallic interface makes it possible to control the SPR response and the sensitivity of the SPR measurements. This should lead to improve performance and sensitivity of the SPR sensors.

Figure 7 shows the plasmonic response variation as a function of the number of graphene layers. This graph shows that the increase of the graphene layer number $L$ leads to a modification and a change of the width of the resonance peaks, which respectively becomes broader, a variation of its amplitude, and a displacement of the resonance peak. For six layers of graphene, the resonance wavelengths go from 536 to 551 nm for a refractive index equal to 1.33. This is justified by Fig. 8 which reflects the variation of the resonance wavelength ranging from 1 to 6 layers of graphene. It is clearly noticeable from this figure that the resonance wavelength $\lambda_{res}$ changes with the number of added graphene layers and with the sensitive medium refractive index following an increasing curve. Therefore, sensor sensitivity rises with increasing graphene layer number. But on the other hand, the resonance peak becomes less selective and the resolution of the biosensor decreases due to the broadening of the resonance peak.

**Table 2** Comparison of the proposed sensor sensitivity with other research study

| References | SPR Sensor | Sensitivity (nm\RIU) | Detection range (RIU) |
|---|---|---|---|
| Shukla et al. [59] (2016) | ITO/ZnO/analyte | 2202 | 1.30–1.37 |
| Nayak and Jha [60] (2017) | Ag/graphene/analyte | 6800 | 1.33–1.37 |
| Sharma and Gupta [44] (2005) | NPs Au/analyte | 1900 | 1.342 |
| Fu et al. [51] (2015) | Au/graphene/analyte | 3400 | 1.33–1.37 |
| Shukla et al. [61] (2015) | Au/ZnO/analyte | 3161 | 1.30–1.37 |
| Kapoor et al. [62] (2019) | ITO/Ag/analyte | 1830 | 1.33–1.37 |
| Sharma et al. [63] (2017) | Au/Pt/analyte | 3571 | 1.30–1.35 |
| Das et al. [64] (2020) | Gold nanoro/SARS-CoV-2 | 111,11 deg.RIU$^{-1}$ | 1.32–1.368 |
| Proposed work | Ag-Au alloy NPs/graphene/analyte | 7100 | 1.30–1.40 |

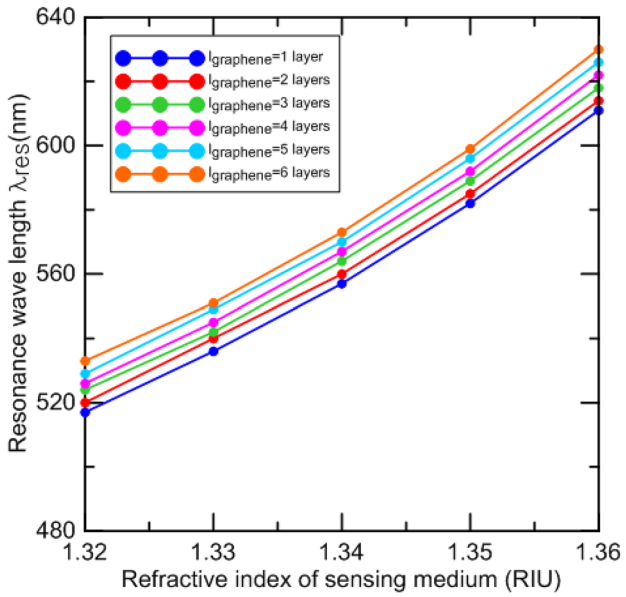


**Fig. 8** variation of $\lambda_{res}$ with the graphene layers number

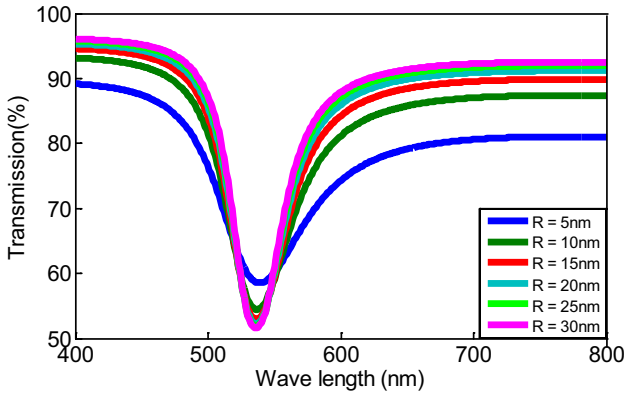


**Fig. 9** Radius effect of Ag-Au spherical nanoparticles on the SPR response of the sensor

Note that the increase in the width at mid-height of the resonance peak as a function of the graphene layers number can be explained by the damping by absorption of the surface plasmons at the interface of the Au–Ag alloy nanoparticle films/graphene, thanks to the optical properties of graphene, especially to the imaginary large part of its refractive index.

Thus, it is necessary to make the best choice for the maximum graphene layer number, which must be set for the good performance of the biosensor. This fixed number should be chosen in order to provide a significant improvement in sensitivity and high detection accuracy. From the two figures, the best performance is obtained for a single layer of graphene, which can be extended up to three layers.

Our findings' results are similar to those found by Fu et al. [51] for a configuration based on a metallic layer of gold. They are in good agreement with the same evolution of the resonance wavelength and the plasmonic response as a function of the graphene layer number for the same detection range (RIU).

Figure 9 shows the effect of the radius of Ag-Au spherical nanoparticles on the plasmon response of the sensor. The curves presented in this figure are obtained by varying the radius of the nanoparticles from 5 to 25 nm and keeping the other parameters constant. According to the figure, the variation in the radius of the nanoparticles leads to a variation in the transmission, the shape of the resonance peak, the full width at half maximum (FWHM), and the resonance wavelength which decreases from 540 to 536 nm passing from a radius of 5 to 25 nm. It can be observed that from a radius of 15 nm, $\lambda_{res}$ stabilizes at 536 nm and the resonance peaks follow the same evolution. In addition, an increase in the nanoparticle size leads to a decrease in the broadening of the SPR curve (FWHM). This is illustrated by Fig. 10 which shows a decreasing curve. This can be explained by Eq. (6) since the damping frequency $\omega_d$ and the radius of nanoparticles are inversely proportional. In fact, when the nanoparticle size increases, $\omega_d$ decreases. Thus, the imaginary part which is responsible for the absorption of the metallic dielectric function decreases. Therefore, this causes a decrease in the transmitted power and the SPR curve should shift downward, when the size of the nanoparticles decreases, which leads to a widening of the curve.

Consequently, the size of the nanoparticles (R) must be taken into account, which is an important parameter acting

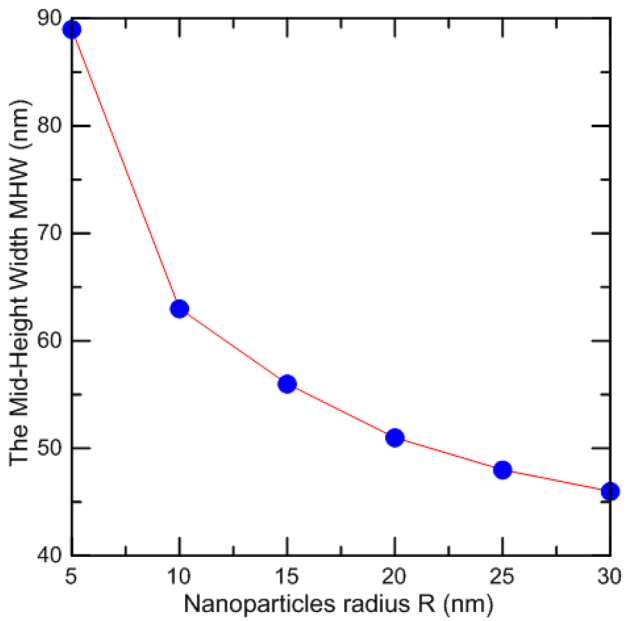


**Fig. 10** Variation of the width at mid-height as a function of the nanoparticle radius

on the sensor performance. The two Figs. 9 and 10 guide us towards an optimal choice of radius. It must be greater than 10 nm. We have chosen 15 nm as the optimal value for this studied configuration.

Let us now move on to study the SPR response of our construct for SARS-COV-2 detection. We employ thiol-attached DNA as a ligand layer because it has been shown to be a good receptor for SARS-COV-2. We gather SARS-COV-2 related data from the literature [13, 14, 54]. Figure 11 presents the transmission variation as a function of the incident wavelength which varies from 400 to 800 nm. The curves are obtained following the numerical simulation without and with SARS-CoV-2, i.e., before and after bonding. It is clearly observed a change of resonance peak (wider) with a displacement towards a higher resonance wavelength which passes from 517 to 543 nm.

The resulting curves reflect the surface plasmons excitation of the metal layer. This can be interpreted by the detection of SARS-CoV-2. Indeed, in the suggested sensing setup, samples taken from human nasopharyngeal swabs are piped in a liquid solution across the sensing channel. When hybridization occurs between SARS-CoV-2 RNA (RdRp-COVID sequence) from a sample with the thiol-attached DNA of receptor molecules, it leads to an important resonance wavelength shift (up to 26 nm). Moreover, the transmission dip is accompanied by a small change in FWHM. This proves the prowess of our conception as a potential plasmonic sensor for the highly sensitive detection of SARS-COV-2.

Figure 12 presents the variation of the resonance wavelength for a series of SARS-CoV-2 solutions having different refractive indices corresponding to the different concentrations. In fact the refractive index of the sample increases with the increase of the concentration or the surface density [14] of SARS-CoV-2 according to Eq. (13). The curve reveals that the increase in the concentration of SARS-CoV-2 leads to an increase in the resonance wavelength, due to the successful recognition and identification of the virus. The limit of detection (LOD) is the minimum change in refractive index that the sensor can detect, i.e the lowest possible concentration that can be detected by the sensor. Therefore, a limit detection of 1.3245, which corresponds to a virus surface density equal to $1 * 10^{13} perm^2$ [14], has been obtained with a good reproducibility.

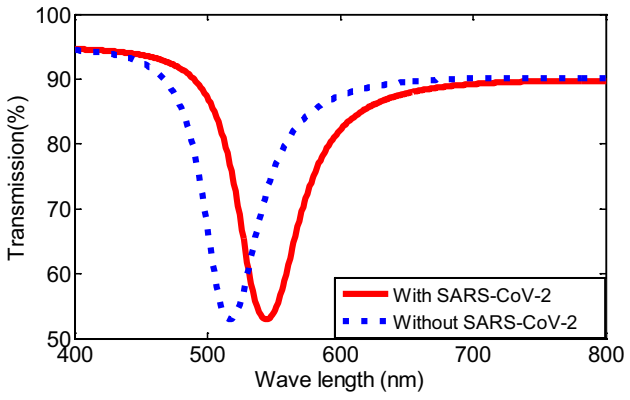


**Fig. 11** SPR curve for SARS-CoV-2 detection

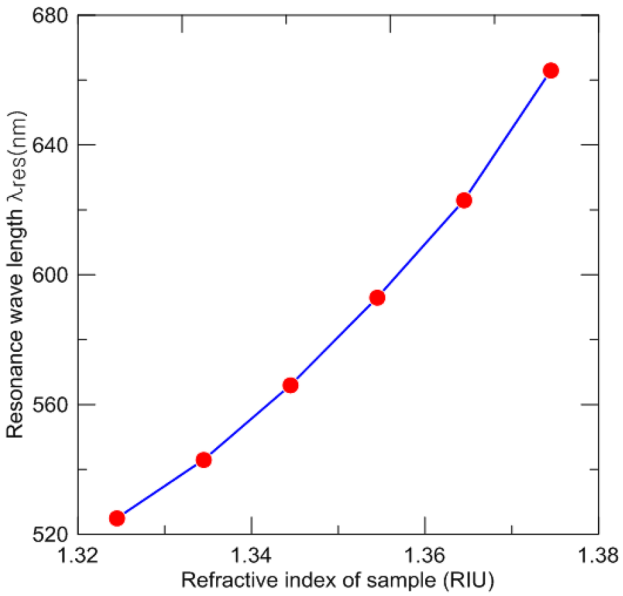


**Fig. 12** Variation of $\lambda_{res}$ as a function of the refractive index of the sample containing SARS-CoV-2

## Conclusions

To take advantage of the benefits of Au–Ag nanoparticles and the interests of graphene, we have combined the two approaches in a single configuration. In this work, an optical fiber SPR sensor based on an Au–Ag alloy nanoparticle films covered by a layer of graphene was theoretically studied. We have successfully shown that the proposed configuration offers better sensitivity and good resolution. A parametric study was subsequently carried out. We have found that the number of graphene layers has a significant influence on the sensitivity and precision of sensor detection. Thus, this number of layers should not exceed three layers to give good performance. Moreover, we have proved that the size of the nanoparticles has an important effect on the transmission spectra and the resolution of the sensor. Hence, the nanoparticle radius should be greater than 10 nm. Finally, the proposed design was tested on the detection of SARS-CoV-2 using the thiol-tethered DNA as a suitable receptor.

**Author Contribution** YS wrote the manuscript text, performed the calculation and prepared the figures. MHG, KM, and MS evaluated the results, contributed to the numerical simulation, and corrected the manuscript text. HB checked the final version of the manuscript and contributed to the interpretation of the figures.

## Declarations

**Ethics Approval** Not applicable.

**Consent to Participate** Not applicable.

**Consent for Publication** Not applicable.

**Competing Interests** The authors declare no competing interests.

## References


1. Li Q et al (2020) Early transmission dynamics in Wuhan, China, of novel coronavirus infected pneumonia New Engl. J Med 382:1199–1207. https://doi.org/10.1056/NEJMoa2001316
2. World Health Organization. (2020) Transmission of SARS-CoV-2: implications for infection prevention precautions. https://reliefweb.int/sites/reliefweb.int/files/resources/WHO-2019-nCoV-Sci_Brief-Transmission_modes-2020.3-eng.pdf
3. Li Z, Yi Y, Luo X, Xiong N, Liu Y, Li S et al (2020) Development and clinical application of a rapid IgM-IgG combined antibody test for SARS-CoV-2 infection diagnosis. J Med Virol 92(9):1518–1524. https://doi.org/10.1002/jmv.25727
4. Egger M, Bundschuh C, Wiesinger K, Gabriel C, Clodi M, Mueller TB et al (2020) Comparison of the Elecsys Anti-SARS-CoV-2 immunoassay with the EDI enzyme linked immunosorbent assays for the detection of SARS-CoV-2 antibodies in human plasma Clin. Chim Acta 509:18–21. https://doi.org/10.1016/j.cca.2020.05.049
5. Dieplinger B et al (2020) Diagnostic value and key features of computed tomography in coronavirus disease 2019 Emerg. Microb Infect 9:787–793. https://doi.org/10.1080/22221751.2020.1750307
6. Yu F et al (2020) Quantitative detection and viral load analysis of SARS-CoV-2 in infected patients Clin. Infect Dis 71:793–798. https://doi.org/10.1093/cid/ciaa345
7. Yan C, Cui J, Huang L, Du B, Chen L, Xue G et al (2020) Rapid and visual detection of 2019 novel coronavirus (SARS-CoV-2) by a reverse transcription loop-mediated isothermal amplification assay Clin. Microbiol Infect 26:773–779. https://doi.org/10.1016/j.cmi.2020.04.001
8. Seo G, Lee G, Kim MJ, Baek SH, Choi M, Ku KB, Lee CS, Jun S, Park D, Kim HG et al (2020) Rapid detection of COVID-19 causative virus (sars-cov-2) in human nasopharyngeal swab specimens using field-effect transistor-based biosensor. ACS Nano 14(4):5135–5142. https://doi.org/10.1021/acsnano.0c02823
9. Abedin S, Kenison J, Vargas C, Potma EO (2019) Sensing biomolecular interactions by the luminescence of a planar gold film. Anal Chem 91(24):15883–15889. https://doi.org/10.1021/acs.analchem.9b04335
10. Bijalwan A, Rastogi V (2018) Gold-aluminum-based surface plasmon resonance sensor with a high quality factor and figure of merit for the detection of hemoglobin. Appl Opt 57(31):9230–9237. https://doi.org/10.1364/AO.57.009230
11. Baccar H, Mejria MB, Hafaiedh I, Ktari T, Aouni M, Abdelghani A (2010) Surface plasmon resonance immunosensor for bacteria detection. Talanta 82:810–814. https://doi.org/10.1016/j.talanta.2010.05.060
12. Béland P, Berini P (2017) Viability assessment of bacteria using long-range surface plasmon waveguide biosensors. Appl Phys A 123(1):31. https://doi.org/10.1007/s00339-016-0625-3
13. Peng X, Zhou Y, Nie K, Zhou F, Yuan Y, Song J, Qu J (2020) Promising near-infrared plasmonic biosensor employed for specific detection of SARS-CoV-2 and its spike glycoprotein. New J Phys 22(10):103046
14. Uddin SM A, Chowdhury SS, Kabir E (2021) Numerical analysis of a highly sensitive surface plasmon resonance sensor for sars-cov-2 detection. Plasmonics 1–13
15. Farre M, Kantiani L, Barcelo D (2007) Advances in immunochemical technologies for analysis of organic pollutants in the environment. Trac Trends Anal Chem 26:1100–1112. https://doi.org/10.1016/j.trac.2007.10.004
16. Dutra RF, Mendes RK, da Silva VL, Kubota LT (2007) Surface plasmon resonance immunosensor for human cardiac troponin T based on self-assembled monolayer. J Pharm Biomed Anal 43:1744–1750. https://doi.org/10.1016/j.jpba.2006.12.013
17. Saylan Y, Akgönüllü S, Çimen D, Derazshamshir A, Bereli N, Yılmaz F, Denizli A (2017) Development of surface plasmon resonance sensors based on molecularly imprinted nanofilms for sensitive and selective detection of pesticides. Sens Actuators B Chem 241(446):454. https://doi.org/10.1016/j.snb.2016.10.017
18. Daniel MC, Astruc D (2004) Gold nanoparticles: assembly, supramolecular chemistry, quantum-size-related properties, and applications toward biology, catalysis, and nanotechnology. Chem Rev 104(1):293–346. https://doi.org/10.1021/cr030698
19. Luo D, Tuersun P (2014) The optimization design for improving film optical transmissivity via the sphere metallic nanoparticles. Optik 125(14):3707–3709. https://doi.org/10.1016/j.ijleo.2014.01.128
20. Brahmachari K, Ray M (2015) Performance analysis of a plasmonic sensor based on gold nanoparticle film in infrared light using the admittance loci method. J Appl Phys 117(8):083110. https://doi.org/10.1063/1.4913604
21. Burda C, Chen X, Narayanan R, El-Sayed MA (2005) Chemistry and properties of nanocrystals of different shapes. Chem Rev 105(4):1025–1102. https://doi.org/10.1021/cr030063a
22. El-Sayed MA (2004) Small is different: shape-, size-, and composition-dependent properties of some colloidal semiconductor nanocrystals. Acc Chem Res 37(5):326–333. https://doi.org/10.1021/ar020204f
23. El-Sayed MA (2001) Some interesting properties of metals confined in time and nanometer space of different shapes. Acc Chem Res 34(4):257–264. https://doi.org/10.1021/ar960016n
24. Hvolbæk B, Janssens TVW, Clausen BS, Falsig H, Christensen CH, Nørskov JK (2007) Catalytic activity of Au nanoparticles. Nano Today 2(4):14–18. https://doi.org/10.1016/S1748-0132(07)70113-5
25. Haruta M (2005) Gold rush. Nature 437(7062):1098–1099
26. Maurya JB, Prajapati YK (2017) Influence of dielectric coating of metal layer in surface plasmon resonance sensor. J Plasmon 12:1121–1130. https://doi.org/10.1007/s11468-016-0366-3
27. Ong BH, Yuan X, Tjin SC, Zhang J, Ng HM (2006) Optimized film thickness for maximum evanescent field enhancement of a bimetallic film surface plasmon resonance biosensor. Sensors and Actuators B 114:1028–1034. https://doi.org/10.1016/j.snb.2005.07.064
28. Wu L, Chu HS, Koh WS, Li EP (2010) Highly sensitive graphene biosensors based on surface plasmon resonance. Opt Express 18:14395–14400. https://doi.org/10.1364/OE.18.014395
29. Gervais T, Tensen KF (2006) Mass transport and surface reactions in microfluidic systems. Chem Eng Sci 61:1102–1121. https://doi.org/10.1016/j.ces.2005.06.024
30. Saad Y, Selmi M, Gazzah MH, Belmabrouk H (2018) Theoretical evaluation of a fiber-optic SPR biosensor based on a gold layer treated with thiol acid. The European Physical Journal Applied Physics 82(3):31201. https://doi.org/10.1051/epjap/2018180059
31. Saad Y, Selmi M, Gazzah MH, Bajahzar A, Belmabrouk H (2019) Performance enhancement of a copper-based optical fiber SPR

sensor by the addition of an oxide layer. Optik 190:1–9. https://doi.org/10.1016/j.ijleo.2019.05.089
32. Islam MS, Cordeiro CM, Sultana J et al (2019) A Hi-Bi ultra sensitive surface plasmon resonance fiber sensor". IEEE Access 7:79085–79094. https://doi.org/10.1109/ACCESS.2019.2922663
33. Saad Y, Selmi M, Gazzah MH, Belmabrouk H (2017) Graphene effect on the improvement of the response of optical fiber SPR sensor. IEEE Sens J 17(22):7440–7447. https://doi.org/10.1109/JSEN.2017.2758258
34. Mak KF, Ju L, Wang F, Heinz TF (2012) Optical spectroscopy of graphene: from the far infrared to the ultraviolet. Solid State Commun 152(15):1341–1349. https://doi.org/10.1016/j.ssc.2012.04.064
35. Shi Z, Yang Y, Gan L, Li Z-Y (2016) Broadband tunability of surface plasmon resonance in graphene-coating silica nanoparticles. Chin Phys B 25(5):057803. https://doi.org/10.1088/1674-1056/25/5/057803
36. Song B, Li D, Qi WP, Elstner M, Fan CH, Fang HP (2010) Graphene on Au (111): a highly conductive material with excellent adsorption properties for high-resolution bio/nanodetection and identification. ChemPhysChem 11(3):585–589. https://doi.org/10.1002/cphc.200900743
37. Rifat AA, Mahdiraji GA, Chow DM et al (2015) Photonic crystal fiber-based surface plasmon resonance sensor with selective analyte channels and graphene- silver deposited core. Sensors 15(5):11499–11510. https://doi.org/10.3390/s150511499
38. Kretschmann E, Raether H (1968) Radiative decay of non radiative Surface plasmons Excited by light, Z. Naturforsch 23:2135–2136. https://doi.org/10.1515/zna-1968-1247
39. Qiu G, Gai Z, Tao Y, Schmitt J, Kullak-Ublick GA, Wang J (2020) Dual-functional plasmonic photothermal biosensors for highly accurate severe acute respiratory syndrome coronavirus 2 detection. ACS Nano 14(5):5268–5277. https://doi.org/10.1021/acsnano.0c02439
40. Shang J, Ye G, Shi K, Wan Y, Luo C, Aihara H, Geng Q, Auerbach A, Li F (2020) Structural basis of receptor recognition by sarscov- 2. Nature 581(7807):221–224. https://doi.org/10.1038/s41586-020-2179-y
41. Nag P, Sadani K, Mukherji S (2020) Optical fiber sensors for rapid screening of COVID-19. Transactions of the Indian National Academy of Engineering 5(2):233–236. https://doi.org/10.1007/s41403-020-00128-4
42. Gupta BD, Kant R (2018) Recent advances in surface plasmon resonance based fiber optic chemical and biosensors utilizing bulk and nanostructures. Opt Laser Technol 101:144–161. https://doi.org/10.1016/j.optlastec.2017.11.015
43. Sharma AK, Gupta BD (2005) Fibre-optic sensor based on surface plasmon resonance with Ag–Au alloy nanoparticle films. Nanotechnology 17(1):124. https://doi.org/10.1088/0957-4484/17/1/020
44. Sharma AK, Gupta BD (2005) Fiber optic sensor based on surface plasmon resonance with nanoparticle films. Photonics Nanostruct Fundam Appl 3(1):30–37. https://doi.org/10.1016/j.photonics.2005.06.001
45. Kreibig U (1974) Electronic properties of small silver particles: the optical constants and their temperature dependence. J Phys F: Met Phys 4(7):999
46. Roy RK, Mandal SK, Pal AK (2003) Effect of interfacial alloying on the surface plasmon resonance of nanocrystalline Au–Ag multilayer thin films. Eur Phys J B 33:109. https://doi.org/10.1140/epjb/e2003-00147-x
47. Link S, Wang ZL, El-Sayed MA (1999) Alloy formation of gold–silver nanoparticles and the dependence of the plasmon absorption on their composition. J Phys Chem B 103:3529. https://doi.org/10.1021/jp990387w
48. Hofmeister H (2009) Shape variations and anisotropic growth of multiply twinned nanoparticles. Z Kristallogr 224(11):528–538
49. Mougin K, Haidara H, Castelein G (2001) Controlling the two-dimensional adhesion and organization of colloidal gold nanoparticles. Colloids Surf, A 193(1–3):231–237. https://doi.org/10.1016/S0927-7757(01)00744-0
50. Ung T, Liz-Marzan LM, Mulvaney P (2001) Optical properties of thin films of Au@ SiO2 particles. J Phys Chem B 105(17):3441–3452. https://doi.org/10.1021/jp003500n
51. Fu H, Zhang S, Chen H, Weng J (2015) Graphene enhances the sensitivity of fiber-optic surface plasmon resonance biosensor. IEEE Sens J 15(10):5478–5482. https://doi.org/10.1109/JSEN.2015.2442276
52. Peterlinz KA, Georgiadis RM, Herne TM, Tarlov MJ (1997) Observation of hybridization and dehybridization of thiol-tethered dna using two-color surface plasmon resonance spectroscopy. J Am Chem Soc 119(14):3401–3402. https://doi.org/10.1021/ja964326c
53. Asghari A, Wang C, Yoo KM, Dalir H, Chen RT (2020) Fast accurate point of care COVID-19 pandemic diagnosis enabled through advanced lab-on-a-chip optical biosensors: opportunities and challenges. arXiv preprint arXiv: 2008. 08572. https://doi.org/10.1063/5.0022211
54. Zhang Q, Zhong L, Tang P, Yuan Y, Liu S, Tian J, Lu X (2017) Quantitative refractive index distribution of single cell by combining phase-shifting interferometry and afm imaging. Sci Rep 7(1):1–10. https://doi.org/10.1038/s41598-017-02797-8
55. Van Manen HJ, Verkuijlen P, Wittendorp P, Subramaniam V, Van den Berg TK, Roos D, Otto C (2008) Refractive index sensing of green fluorescent proteins in living cells using fluorescence lifetime imaging microscopy. Biophys J 94(8):L67–L69. https://doi.org/10.1529/biophysj.107.127837
56. Wölfel R, Corman VM, Guggemos W, Seilmaier M, Zange S, Müller MA, Niemeyer D, Jones TC, Vollmar P, Rothe C et al (2020) Virological assessment of hospitalized patients with covid- 2019. Nature 581(7809):465–469. https://doi.org/10.1038/s41586-020-2196-x
57. Anower MS, Rahman MS, Rikta KA (2018) Performance enhancement of graphene-coated surface plasmon resonance biosensor using tungsten disulfide. Opt Eng 57(1):017114. https://doi.org/10.1117/1.OE.57.1.017114
58. P. Yeh P (1988) Optical waves in layered media. John Wiley and Sons, New York, pp 102–117.https://doi.org/10.1063/1.2810419
59. Shukla S, Sharma NK, Sajal V (2016) Theoretical analysis of surface plasmon resonance based fiber optic sensor using ITO and ZnO thin films. Opt Quant Electron 48(1):57. https://doi.org/10.1007/s11082-015-0351-7
60. Nayak JK, Jha R (2017) Numerical simulation on the performance analysis of a graphene-coated optical fiber plasmonic sensor at anti-crossing. Appl Opt 56(12):3510–3517. https://doi.org/10.1364/AO.56.003510
61. Shukla S, Sharma NK, Sajal V (2015) Sensitivity enhancement of a surface plasmon resonance based fiber optic sensor using ZnO thin film: a theoretical study. Sens Actuators, B Chem 206:463–470. https://doi.org/10.1016/j.snb.2014.09.083
62. Kapoor V, Sharma NK, Sajal V (2019) Indium tin oxide and silver based fiber optic SPR sensor: an experimental study. Opt Quant Electron 51(4):125. https://doi.org/10.1007/s11082-019-1837-5
63. Sharma NK, Shukla S, Sajal V (2017) Surface plasmon resonance based fiber optic sensor using an additional layer of platinum: a theoretical study. Optik 133:43–50. https://doi.org/10.1016/j.ijleo.2017.01.004
64. Das CM, Guo Y, Yang G, Kang L, Xu G, Ho HP, Yong KT (2020) Gold nanorod assisted enhanced plasmonic detection scheme of COVID-19 SARS-CoV-2 spike protein. Advanced theory and simulations 3(11):2000185. https://doi.org/10.1002/adts.202000185